AD-A124 792 DESIGN OF CHOKING CASCADE TURNS(U) AIR FORCE INST OF TECH WRIGHT-PATTERSON AFB OH SCHOOL OF ENGINEERING J BAIRD DEC 82 AFIT/GAE/AA/82D-3 1/1

UNCLASSIFIED F/G 16/4.1 NL

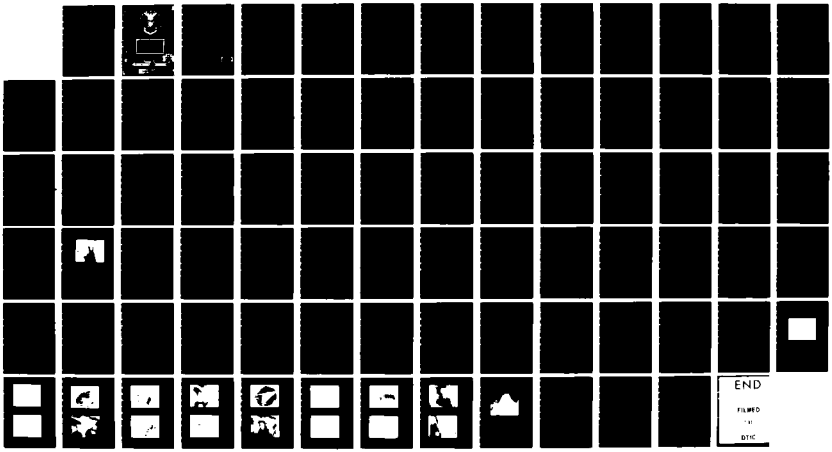

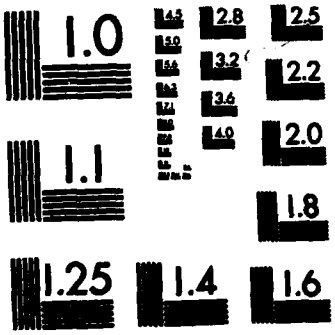

MICROCOPY RESOLUTION TEST CHART
NATIONAL BUREAU OF STANDARDS-1963-A

AD A124792

DESIGN OF CHOKING

CASCADE TURNS

THESIS

AFIT/GAE/AA/82D-3 Jason Baird

Capt USAF

DTIC
ELECTE
FEB 23 1983
S D
E

Approved for public release; distribution unlimited

AFIT/GAE/AA/82D-3

DESIGN OF CHOKING CASCADE TURNS

THESIS

Presented to the Faculty of the School of Engineering

of the Air Force Institute of Technology

Air University

in Partial Fulfillment of the

Requirements for the Degree of

Master of Science

DTIC COPY INSPECTED 2

Accession For	
NTIS GRA&I	☒
DTIC TAB	☐
Unannounced	☐
Justification	
By	
Distribution/	
Availability Codes	
Dist	Avail and/or Special
A	

by

Jason Baird, B.S.

Capt USAF

Graduate Aeronautical Engineering

December 1982

Approved for public release; distribution unlimited

Preface

Ramjet engines are being considered by both the Air Force and Navy for tactical air launched missile propulsion. Designs for both services require the ducting of inlet airflow into the ramjet combustor in a particular direction dictated by the combustor design. The designs require a venturi array, or aerodynamic grid, in the inlet to control flow into the combustor under supercritical inlet operating conditions. Added to this is the problem that the inlet(s) may be located away from the missile centerline, while the optimum position for the ramjet engine may be coaxial with the missile, requiring turning the inlet flow from its original direction. A research project was proposed by Mr. David B. Wilkinson, an aerospace engineer with the Ramjets Division of the Air Force Wright Aeronautical Laboratory (AFWAL/PORA), to combine flow alignment, turning, and distortion control functions into a single cascade of aerodynamically-shaped guide vanes. If this could be done, reductions in the propulsion system weight and volume, as well as improved inlet pressure recovery, could be expected. This thesis applies the hydraulic analogy and flow visualization using the AFIT 40-inch water table to study the feasibility of different cascade designs.

I want to thank Mr. Wilkinson for his ideas and assistance throughout my study. Also, I would like to thank Mr. Carl Shortt and Mr. Jack Tiffany of the AFIT Shops for

their excellent work in the construction of the different cascades used in my study. I would like to thank Dr. Elrod for his guidance during my study, without which there would have been no worthwhile work done. Most of all, I thank my wife, Barbara, and my son, Ian, for the support they gave me during my thesis work.

Contents

Preface i

List of Figures v

List of Tables vii

List of Symbols viii

Abstract x

I. Introduction 1

Background 1
Objectives of Study 2
Scope of Study 2

II. Theory 4

Inlets 4
Aerodynamic Grid 6
Flow Turning 7
Improved Turning 12
Hydraulic Analogy 13

III. Design of Shock Postioning Cascade Turns 16

Reynolds Number 16
Throat Mach Number 17
Vane Design 17
Summary 19

IV. Procedure 21

Set-Up and Photography 21
Flow Control Tests 22

V. Experimental Equipment and Methods 24

Water Table 24
Test Sections 24
Cascades 25
Optics 26
Depth Measurements 27

VI. Results 28

Shock Positioning 28
Pressure Recovery 28
Radius Ratio 31
Wall Shape 32
Solidity and Blockage 32

Cascade Diffusion Angle 33
Angle-of-Attack 33
Pipe Flow 34

VII. Conclusions and Recommendations 35

Conclusions 35
Recommendations 36

Bibliography 37

Appendix A: Cascade Design 38

Appendix B: Vane Cross-Sections 42

Appendix C: Pipe Flow Analysis 50

Appendix D: Photographs 55

List of Figures

Figure

1 Choking Cascade Turn 5

2 Missile Inlet Ducting 9

3 Miter Turn with Turbulence Zones 10

4 Miter Turn 11

5 Diffuser Oblique Shock 29

6 Cascade Diffusion Angle 34

A-1 Vane Layout 41

B-1 Cascade 1 44

B-2 Cascade 2 45

B-3 Cascade 3 46

B-4 Cascade 4 47

B-5 Cascade 5 48

B-6 Aerodynamic Grid 49

C-1 Flow Chart of Pipe Flow Calculations 51

D-1 Cascade 1, Optimum Inlet Pressure Recovery 55

D-2 Cascade 1, Cascade Choked 56

D-3 Cascade 2, Optimum Inlet Pressure Recovery 56

D-4 Cascade 2, Cascade Choked 57

D-5 Cascade 2 From Above, Showing Vertical Flow Accelerations 57

D-6 Cascade 3, Optimum Inlet Pressure Recovery 58

D-7 Cascade 3, Cascade Choked 58

D-8 Cascade 3 From Above, Showing Vertical Flow Accelerations 59

D-9 Cascade 4, Optimum Inlet Pressure Recovery 59

D-10 Cascade 4, Cascade Choked 60

D-11 Cascade 4 From Above, Showing Vertical Flow Accelerations 60

D-12 Cascade 5, Optimum Inlet Pressure Recovery 61

D-13 Cascade 5, Cascade Choked 61

D-14 Grid, Optimum Inlet Pressure Recovery 62

D-15 Grid Choked 62

D-16 Grid From Above, Showing Hydraulic Jumps 63

D-17 Normal Hydraulic Jump in Inlet 63

D-18 Experimental Set-Up 64

List of Tables

Table

I Hydraulic Analogy Relations 15

II Comparisons and Performance of Cascade Designs 30

C-I Calculated Static Pressure Ratios 54

List of Symbols

A - Area

A_s - Speed of sound in air

B - Cascade inlet height

C - $\sqrt{GD}$

D - Water depth

D_o - Depth of water head

D_h - Hydraulic diameter

F - Froude number

G - Acceleration of gravity, 32.17 ft/s

H - Distance between vane centers of curvature

K - Ratio of specific heats

L - Characteristic Length

l - Vane chord length

M - Mach number

m - Distance across turn, along the line of bending

n - Number of vanes

P - Static pressure

P_o - Stagnation pressure

R - Radius

R_e - Reynolds number

R_g - Gas constant for air

S - Cascade throat height

T - Static temperature

V - Velocity

ρ - Static density

A-O-A - Angle-of-attack

ν - Kinematic viscosity

θ - Angle of turn

ε - Surface roughness

$4f$ - D'Arcy friction factor

Abstract

Five different shock-positioning cascades, for short-radius turns in ramjet inlet diffusers, were selected, designed, and tested on the AFIT water table. These flow controllers were to perform the same function as the conventional arrangement of an aerodynamic grid and a long-radius turn. The tests were to determine the suitability of the water table for such experimentation, in addition to determining the flow-control capabilities and pressure recovery of the cascades. All five designs accomplished the flow-control function as designed, and two designs exhibited the same or better pressure recovery than an aerodynamic grid, in the water table tests. The water table proved to be an excellent means of testing these cascades, primarily due to the ease of flow visualization in the test zone. The shock-positioning cascade, short-radius turn concept shows promise and should be tested further in gas-dynamic apparatus.

I. Introduction

Background

Ramjet engines are under consideration for use in tactical air-to-air missiles, because of advantages they offer over the solid-propellant rocket engines currently used. Some of the designs require ducting of the incoming air flow to a combustor on an axis different from that of the vehicle inlet. Also, some designs require a venturi array (or aerodymanic grid) downstream of the vehicle inlet and forward of the combustor, to control the inlet internal shock position. The current designs use a large radius turn plus a grid to turn the flow and position the shock. This research was a study of the combination of an abrupt vaned miter, or short radius, turn with an aerodynamic grid, resulting in reduced weight and volume and improved pressure recovery compared to the current designs.

Ramjets operate most efficiently in the supersonic flight regime, because they have no mechanical air compressors and must rely on shock-wave compression of air. Conventional ramjets burn a fuel and air mixture which must be subsonic to maintain combustion. Accordingly, an inlet must optimize the means of producing shocks to compress the air and slow it down before it enters the combustor. This flow conditioning is done by shocks ahead of the inlet, in the inlet, and in the diffuser which follows immediately after the inlet. Supercritical inlet operation is the

optimum for pressure recovery and stability of the inlet shock system. It is the function of the aerodynamic grid to maintain supercritical operation, by isolating the inlet shock system from pressure variations in the combustor.

Large radius turns in the diffusers of current designs are used to duct the airflow because such turns have better pressure recovery than abrupt, unvaned short radius turns. The inclusion of turning vanes in a short radius turn improves the pressure recovery. The combination of vanes and an aerodynamic grid into one cascade should allow air flow turning and shock control with a reduction of weight and volume (compared with the present design approach), and with maximum pressure recovery.

Objectives of Study

The primary objective of this study was to investigate various combinations of turning vanes with an aerodynamic grid, to see if airflow turning and inlet shock positioning functions could be combined into one cascade. Additionally, the applicability of the hydraulic analogy to studies of this type was investigated.

Scope of Study

The principles involved in inlet operation and efficient airflow turning were researched in depth, to gain an understanding of the mechanics of aerodynamic grid and turning vane operation. The hydraulic analogy was

investigated, and then used to test models of various cascade designs. Photographs were taken of water flow through the cascades under different conditions, as an aid in visualization of boundary layers, flow separation, and hydraulic jumps. The study was intended to be the initial step in the development of shock positioning cascade turns; therefore, it did not involve gas dynamic tests of cascade models.

II. Theory

In order to develop cascade designs and water table tests, it was necessary to investigate the principles associated with supersonic inlets, aerodynamic grids , flow turning in ducts, and the hydraulic analogy. External shock inlets were the only kind of inlet considered in this study.

Inlets

External shock inlets operate in three modes: subcritical, critical, and supercritical. A normal shock is forward of the inlet lip in subcritical operation, a mode associated with flow spillage around the lip (see Figure 1). The spillage causes increased drag and reduced thrust when compared to critical operation. Critical operation is the condition when a normal shock occurs at the inlet lip and there is no spillage. Supercritical operation occurs when the normal shock is downstream of the inlet lip. There is no spillage, but the shock is formed at a point where the cross-sectional area is larger than that for critical operation, and the shock occurs at a higher Mach number. This results in greater energy losses across the shock than for critical operation. However, this mode is more stable than critical operation, as it takes more downstream back pressure change to eject the shock forward out of the inlet (Ref 3: 213-214). The position of the normal shock is determined by downstream flow restrictions, so it is

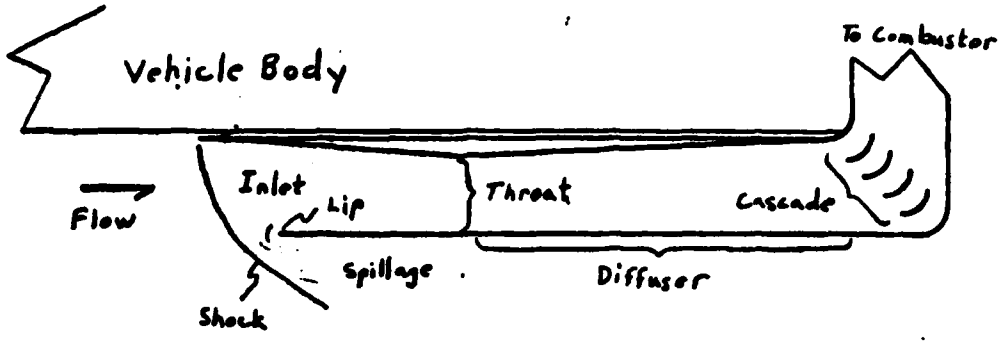

Chin-Type Inlet; Subcritical Operation

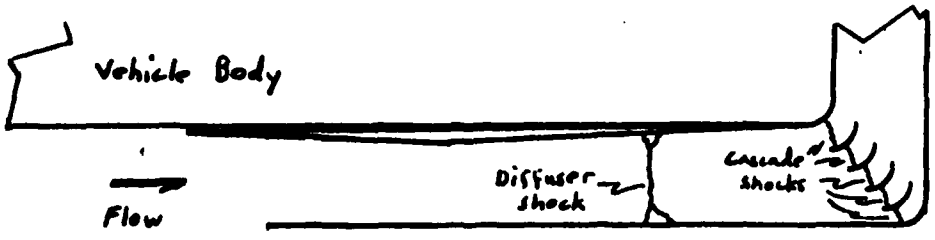

Same Inlet; Supercritical Operation. Note the Shocks Due to the Onset of Choking of the Cascade.

Figure 1 Choking Cascade Turn

sensitive to variations in exhaust-nozzle area and fuel flow rate. So, most ramjet inlet-diffuser combinations are designed to operate supercritically.

Efficient combustion of a fuel-air mixture requires control of the flow velocity profile across the diffuser. Fuel is injected into the flow immediately after the diffuser, and the flow velocity profile should be as uniform across the injectors as possible. A uniform velocity profile also allows the flow to be tailored by flame-holders into the optimum flame geometry for the system. This profile control requires positioning the normal shock forward in the vehicle inlet during supercritical operation - almost to the point of critical operation. If the shock is too far downstream, a boundary layer of slower or stagnant flow builds along the diffuser walls, in association with and downstream of the shock. The farther downstream the shock, the thicker the boundary layer. The flow velocity in the central region of the diffuser becomes much greater than that of the region closer to the walls, and this great nonuniformity causes a nonuniformity in the fuel-air ratio and a disturbance of the flame geometry. These factors often result in inefficiency or loss of combustion, and are the reasons the aerodynamic grid was developed (Ref 10: 3-4) (Ref 7: 135). A properly designed aerodynamic grid will produce a uniform velocity profile.

Aerodynamic Grid. The aerodynamic grid is a flow controller positioned aft of the diffuser and forward of the

combustor in a ramjet engine. It consists of a grid of short venturis, designed so that the flow through them is subsonic when the diffuser normal shock is at or just inside the vehicle inlet entrance. As the inlet flow velocity increases, (due to a transient combustion instability, or to throttling the engine) and the normal shock moves downstream, flow in the venturis chokes when the mass flow through them increases to the point of oblique shock formation in the vehicle inlet, and boundary layer separation in the diffuser (Ref 10: 4-5). The farther downstream in the diffuser that a normal shock is positioned, the stronger the shock, and the greater the energy loss across it.

A grid creates increasing back pressure as the pressure in the combustor drops. This increased back pressure holds the diffuser shock forward, thereby improving the diffuser pressure recovery. The flow losses in a properly designed grid are offset by a reduction in the energy loss that otherwise would occur across the diffuser shock if it were farther downstream (Ref 10: 2,3,5).

Flow Turning. In some ramjet applications, the inlet is not on the same axis as the vehicle. One such inlet is envisioned in this work. The inlet is usually chosen to avoid the masking of seekers or warheads in the forward part of the vehicle, in the cases where a ramjet is mounted in the vehicle body.

In this study, the inlet was a scoop, mounted next to

the vehicle body. The combustor and nozzle were mounted in the vehicle body, necessitating turning the flow from the inlet to the combustor (because the inlet and the combustor were on different axes). It is desireable to turn the flow with a good pressure recovery, and the turning may be done by a diffuser duct of either short or long radius. A long radius turn has the best pressure recovery, but necessitates a longer flow passage, and therefore more wall friction losses than in a short radius turn. Also, the longer inlet would be heavier, and it might obstruct the seeker and/or warhead. However, a properly designed set of guide vanes in the miter turn can reduce the energy losses, and make the performance of the turn competitive with the long radius turn (see Figure 2).

Fluid flow around an unvaned miter turn is accompanied by a change in the cross-sectional velocity profile of the fluid, by a spiralling motion of the fluid, and by fluid turbulence in the bend and further downstream (Ref 6: 203). There are two main turbulent zones in a miter turn with smooth walls. One is next to the outside wall, and the other is on the inside wall immediately after the turn (see Figure 3) (Ref 11: 2). Centrifugal force, on the fluid particles as they go around the turn, causes an increase in pressure that forces their velocity to almost zero near the outer wall. The flow separates, and eddys result. Fluid inertia and low fluid velocity, due to shear forces near the inner wall of the turn, cause flow separation from the inner

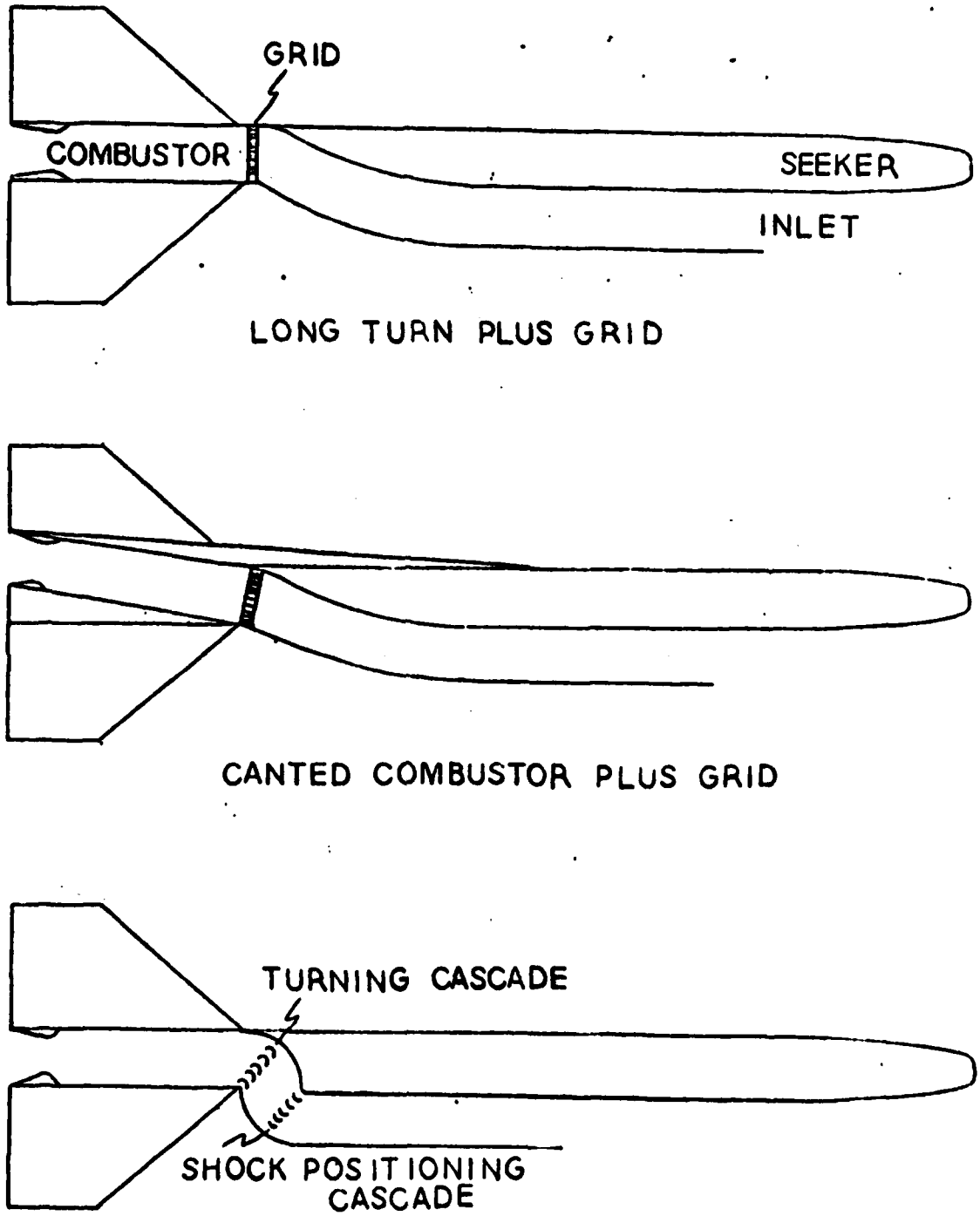

Figure 2 Missile Inlet Ducting

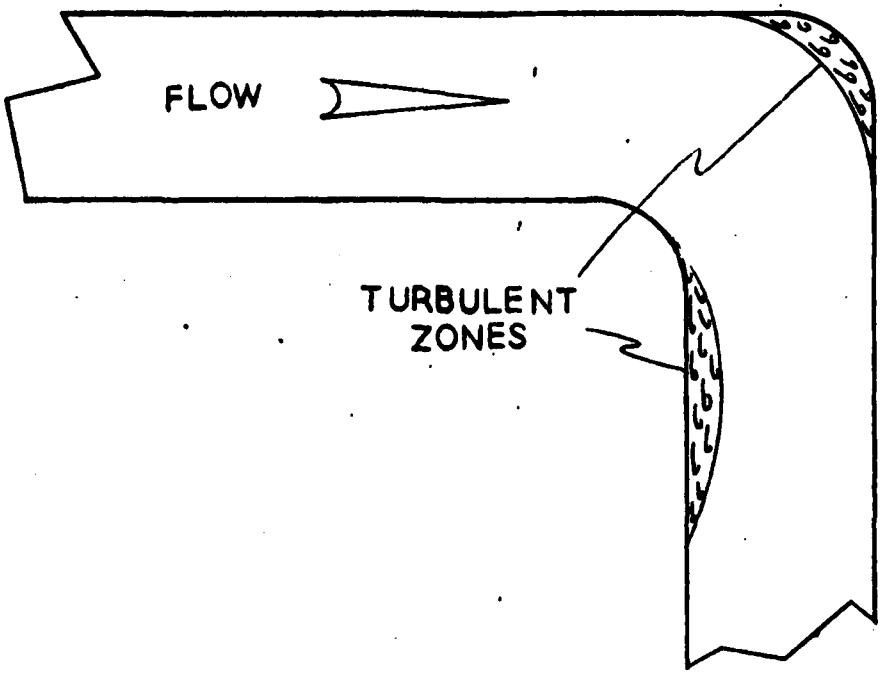

Figure 3 Miter Turn with Turbulent Zones

wall immediately after the turn (Ref 6: 203). This pressure gradient across a turn also causes a twin eddy in the fluid (see Figure 4a). The pressure is low near the inner wall, it increases with radial distance across the bend, and then it rapidly drops off as the separated region near the outside wall is approached (see Figure 4b). This reduction in pressure causes an outward motion of the fluid, which turns into a double spiral through the turn. All this extra fluid motion adds to the friction losses, and creates more downstream turbulence in the fluid (Ref 6: 203-204).

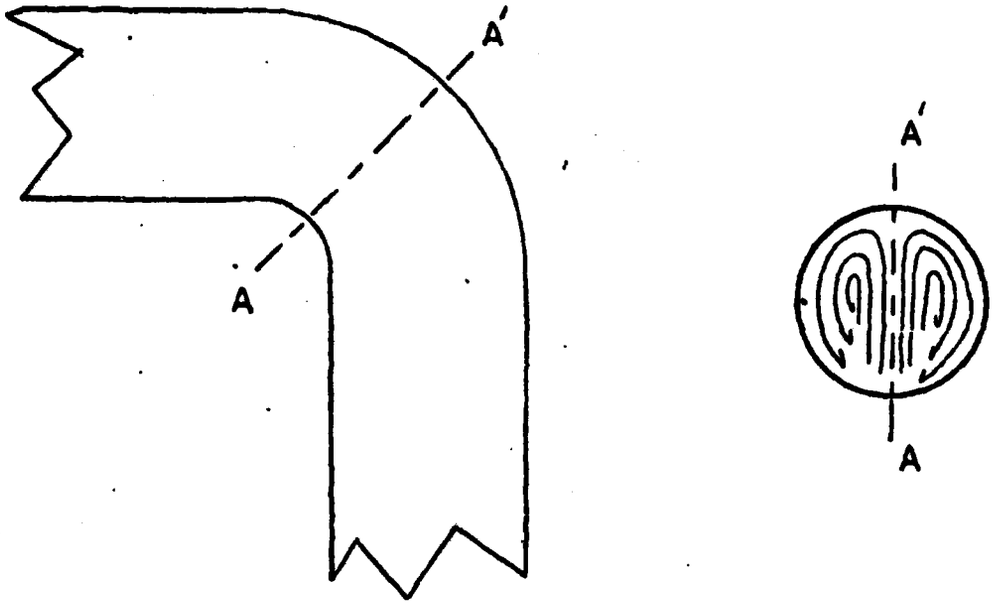

A) Twin Eddy in Turn

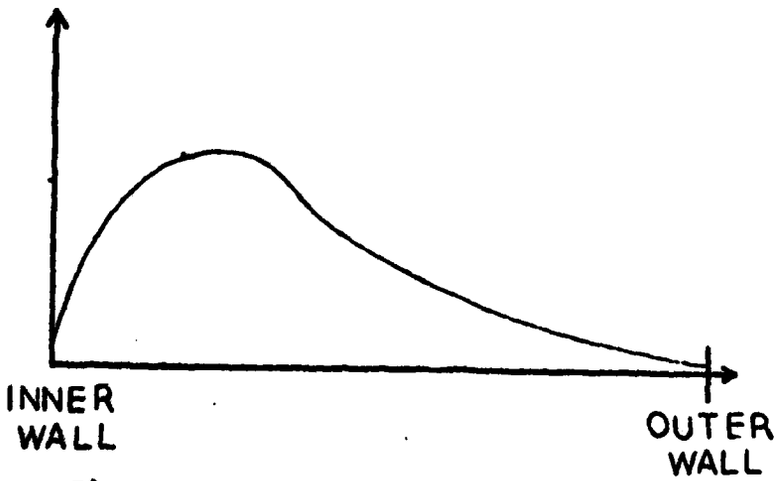

B) Pressure Gradient Across Elbow

Figure 4 Miter Turn (Ref 6: 204)

Improved Turning. What can be done to reduce the losses in a miter turn? The introduction of guide vanes, or splitters, into the turn divides the turn channel into passages with larger radius and aspect ratios, and improves the pressure recovery. The radius ratio of a passage is its radius of curvature divided by its hydraulic diameter (for a rectangular passage, the hydraulic diameter is four times the cross-sectional area, divided by the wetted perimeter). The aspect ratio (for rectangular passages) is the width of the short side of a passage, divided by the length of its long side. The flow resistance of a passage is affected inversely by these two ratios, as might be expected from the above explanation of flow losses. Insertion of guide vanes into a miter turn changes it from a short radius turn to a number of long radius turns with larger radius and aspect ratios, when the radius of curvature of each vane is the same as the radius of curvature of the inner wall of the turn (Ref 4: 372).

Designing the guide vanes with airfoil cross-sections introduces desirable effects. Such an aerodynamic cascade combines the good radius and aspect ratios of guide vanes with stream deflection toward the inner wall of the turn by downwash from the airfoils. When the proper vane angle-of-attack is selected, this deflection prevents flow separation from the inner wall of the turn. A well-designed cascade reduces elbow flow resistance and improves the velocity distribution after the elbow.

For a uniform velocity profile after the turn, an optimum gap-to-chord ratio is 0.3 to 0.4 for water flow (Ref 11: 4). The gap-to-chord ratio is the ratio of the diameter (or height) of the smallest part of the flow passage between two adjacent vanes, to the vane chord length. As the gap-to-chord ratio is reduced, the radius and aspect ratios are increased and the pressure drop will decrease, until the wall friction losses caused by blockage increases enough to offset the drop (Ref 4: 373).

Hydraulic Analogy (Ref 1)

The hydraulic analogy allows the modeling of a gas flow system with a water flow system at a substantially lower velocity than that of the gas. It is a two-dimensional analogy to a two-dimensional gas flow, which mathematically relates certain parameters in water flow to other parameters in a gas flow. The models used in the analogy are usually less expensive than gas flow models, and the test costs are less than wind tunnel test costs. It is not a complete analogy; however, the hydraulic analogy is good for trying out and refining new ideas before gas dynamic work is done.

The assumptions involved in the analogy must be kept in mind when using it. The water flow is assumed to be two-dimensional, which only allows for negligible accelerations in the third dimension. The gas dynamic situation being modeled is assumed to be inviscid, isentropic, two-dimensional, and to have a ratio of specific

heats (k) of 2.0. This last assumption produces some error when the gas is air, but the error is small when considered with the errors introduced by the other assumptions. For air, with k=1.4, the error in P/P_0 computed with k=2.0 is less than 5% at a Mach number of 0.5, and less than 20% up to Mach 3.0.

Water height measurements were the bases for the comparisons between water and air flows in this paper. Height measurements were used to compute gas pressure ratios, Mach numbers, and gas velocities, according to the relations in Table I. In the table, corresponding relationships for air and water flows are located on the same lines, in their appropriately labeled columns.

One design factor that cannot usually be matched in the hydraulic analogy is Reynolds number (see Appendix A). Even though Reynolds numbers are not usually matched, water table models are very good for flow visualization purposes. A slow water flow, from 0 to about 5.0 ft/s, corresponds to airflow up to Mach 3.0. Dye may be injected into the water to study flow separation, streamlines, and turbulence. Hydraulic jumps, which are sudden increases in water depth, form close to points where shocks would form in a gas dynamic flow. Jumps are a very graphic means of supersonic flow visualization that are visible without complex optical systems. The water depth increase across a jump is analogous to the increase in pressure across a shock wave.

Table I

Hydraulic Analogy Relationships

(Ref 1: Table I)

Gas Dynamics	Hydrodynamics
T_2/T_1	D_2/D_1
ρ_2/ρ_1	D_2/D_1
P_2/P_1	$\left(D_2/D_1\right)^2$
$A_s=\sqrt{KR_gT}$	$C=\sqrt{GD}$
$M=\frac{V}{A_s}$	$F=\frac{V}{C}$
$M=\left[\frac{2}{K-1}\right]^{1/2}\left[\left(\frac{P_o}{P}\right)^{\frac{K-1}{K}}-1\right]$	$F=2^{1/2}\left[\frac{D_o}{D}-1\right]^{1/2}$
	$D_o=D\left[\frac{F^2}{2}+1\right]$

III. Design of Shock Positioning Cascade Turns

Reynolds Number

Research on aerodynamic grids has shown that the distribution of the flow exiting an aerodynamic grid does not generally depend on the grid pattern, if the orifices are "small" in relation to the duct cross-sectional area at the grid position. This should be true for flow-turning grids, too, as the flow distribution at their exits would depend on the size of the jets from each orifice. A lower limit on the orifice size, based on the minimum cross-sectional dimension of the orifice, is a Reynolds number of about 100,000 (Ref 9: 7). The orifice size also determines the minimum distance that the grid may be placed forward of the combustion chamber. The larger the openings, the larger the spikes of higher-velocity flow in the grid exit velocity distribution, and the longer the flow passage will have to be between the grid and the combustor to allow enough mixing to reduce the spikes for a uniform velocity profile in the flow entering the combustor. The exact distance is specific to the design, and must be determined experimentally (Ref 10: 4). In the case of this study, the flow blockage of a grid used in a current ramjet design was used as a baseline. The grid has approximately 44% of the flow blocked, figured by dividing the total grid orifice cross-sectional area by the cross-sectional area of the duct at the grid position, and subtracting the resulting ratio

from one.

The Reynolds number of the water table models could not be matched to the Reynolds numbers expected in actual engine operation, for the reasons given in Appendix A.

Throat Mach Number

A cascade should have good pressure recovery when the diffuser is operating critically, as this is the optimum engine operating condition. According to a research report (Ref 9: 3), the cascade throat Mach number should be 0.5 to 0.6 when the diffuser is operating critically, for a good compromise between pressure loss and effectiveness in controlling the mass flow into the combustor. On the other hand, a cascade should choke when the flow through it accelerates to the point of oblique shock formation in the diffuser. The solidity (the ratio of a vane chord to the separation between vanes) of the cascades was chosen so that the orifices choked at a maximum upstream Mach number of 0.465 (Ref 9:3). This value of Mach number was chosen because it had been used in aerodynamic grid tests to maintain inlet shocks in their desired positions.

Vane Design

For liquids, the pressure recovery of a vaned miter turn is optimized in the 2.22 to 4.0 range of cascade solidity (Ref 4: 373). In air, a compressor cascade usually has a solidity of about 1 (Ref 3: 267). The solidity of the

reference grid is approximately 1.5. Two solidities were chosen for the models in this study, one on each end of the spectrum (see Table II). It was decided to design the models this way because of the apparent requirement of different solidities for water and for air. The testing was to be done in water, and the actual use of cascades in engines is with air flow. The required solidity has an effect on the geometry of the vanes, when coupled with the requirement for a specific size for mass flow control. A large solidity, as opposed to a smaller one, will give a relatively small pressure drop around a corner, due to the corresponding relatively large radius and aspect ratios. However, a large solidity also gives greater losses due to increasing channel blockage (Ref 4: 373). Larger solidity leads to less aerodynamic lift on each vane, so the adverse pressure gradients along the suction sides of the vanes are reduced. The flow is less likely to separate (Ref 3: 267). With these concepts, each solidity has to be experimentally chosen for a specific application.

If, during testing, it is seen that the turbulent zone next to the inside wall immediately after the turn still exists with the cascade in place, the angle-of-attack of each vane can be increased until the zone disappears (Ref 11: 10). This increase may also lead to increased flow separation and energy loss for each vane. Once again, this should be considered during experimentation, as it cannot be easily predicted.

Some of the cascade vane forebodies used in this study were designed so that the passages between vanes formed the converging parts of converging-diverging nozzles. The remainder of the forebodies were designed for smooth flow turning in the cascade passages, so the performances of the resulting cascades could be compared to the performances of cascades designed with the other philosophy. The vane forebodies are working in a favorable pressure gradient, so is it is not necessary to use them to form passages according to an area ratio (as in a nozzle). It should be possible to vary the forebody shapes to have the best vanes for good cascade pressure recovery during unchoked cascade operation. However, the vane forebodies are also always working in subsonic flow, and a blunt forebody which was not designed for a smooth flow-passage area reduction might cause abrupt flow re-adjustments. These flow re-adjustments would be due to the abrupt change in duct cross-sectional area (from the area just forward of the cascade to the cascade entrance), and could send pressure disturbances forward in the subsonic flow, into the vehicle diffuser, which would interfere with the inlet shock.

Summary

The models used in this study were designed with solidities of 1.59 to 3.03, in an attempt to show which end of a solidity range of 1.5 to 4 gave the best cascade pressure recovery. Three of the models were constructed so

their individual vane angles-of-attack could be varied from 0° to $+10^\circ$. The models were designed for a cascade inlet area to cascade throat area ratio that caused the cascades to choke when the Mach number at the cascade inlet reached 0.465. This condition also resulted in a cascade throat Mach number of 0.5 to 0.6 when the vehicle diffuser was operating critically, as stated in Reference 9 and verified experimentally during this study.

IV. Procedure

Set-Up and Photography

A combination of wood blocks to simulate the desired flow conditions into and out of the cascade were set-up on the table surface. Two different types of set-ups were used. With one, the exact flow conditions through the cascade were of concern for depth measurements and photographs. With the other type, over-all flow visualization was the concern, so blocks were set-up in an attempt to simulate a ramjet inlet. The latter set-up was used to visually check the cascade performance in the flow-control area, rather than checking pressure loss and specific Mach numbers. This points out some of the good qualities of water table experimentation; many different flow conditions can be set-up and checked quickly, inexpensively, and relatively easily.

The optics were positioned, with the cascade being tested in the light beam, so that the area of interest could be observed. Photographs were taken of the flow through the cascade at each test condition from below the water table. Under some conditions, pictures were also taken from above the table of the flow through the cascade being tested, and of the entire test set-up. The pictures were taken as an aid in flow visualization, and to point out any previously unobserved phenomena. The pictures can be found in Appendix D.

Flow Control Tests

The flow control qualities of cascades, as visualized on the water table, were judged in three ways. The first way was by visually confirming the flow pattern around a cascade with and without dye injected into the flow. The flow control tests were done with a hydraulic jump in the inlet to simulate a shock for the inlet's supercritical operating condition. The next method was to measure water depths at different positions in and around a cascade to find the Froude numbers at those positions, and then to adjust the back pressure seen by the model until the desired Froude numbers were produced. In some instances, the measurements were not taken inside the cascade passages, as it was judged that the turning flow had enough vertical acceleration to invalidate the hydraulic analogy in the passages. That lead to the last method of determining flow control qualities. When vertical accelerations would not allow direct measurement to see if a Froude number of one had been reached in the cascade, signifying choked flow, shadowgraph and direct visual observations were used to confirm or deny the existence of a hydraulic jump downstream of the cascade throat. The hydraulic jump under these conditions is indicative of the presence of a normal shock in gas dynamic flow (boundary layer effects are disregarded) in Shapiro's regime II (Ref 7: 140,141), developed in an analysis of the operating conditions of converging-diverging nozzles. In this regime, the flow rate is independent of the back

pressure. So, if a hydraulic jump was observed in the cascade, downstream of the cascade throat, the cascade was operating in one of this regime, and considered choked.

V. Experimental Equipment and Methods

Water Table

The water table was used to study flow characteristics through different cascades, by way of the hydraulic analogy.

The AFIT water table has a test area of plate glass, 4 ft wide and 8 ft long, lying horizontally between two reservoirs. Water from the head reservoir flows through two filters, one of cheesecloth and the other of metal screen, into the test section. The screens filter out small particles, and smooth the water flow for a more uniform velocity profile at the head of the test section. Exiting the test section, the water passes over a weir whose height may be adjusted by the table operator. The water then enters a receiving tank, where it is recirculated by means of a pump and valves back into the head tank.

The water depth may be controlled by adjusting the weir height, and/or by using the valves to control the pump output (the water head in front of the model).

Test Sections

Two-dimensional wooden nozzles were used to simulate the engine inlet, so the flow conditions into the cascade could be adjusted as desired. Moving the forward ends of the inlet blocks closer together or farther apart varied the flow velocity into the cascade from a simulated low subsonic

to supersonic forward of simulated shocks, depending on the back pressure. Straight-walled blocks were used to make a parallel-walled channel downstream of the cascade being tested. Various blocks were used as plugs in this channel to control the back pressure seen by the vanes.

Cascades

Five different cascades, all constructed by the AFIT shops, were constructed of cast epoxy resin and Plexiglas in the following manner. First, a wood plug was shaped to an airfoil with the desired cross-section. Then, a two-piece Fiberglas mold was laid-up around the airfoil. The mold was coated with a separator (to facilitate removal of the casting), bolted together, and filled with the liquid epoxy mixture. After the epoxy had set-up, the mold was removed, and the epoxy airfoil was sanded to the desired surface finish and painted flat black. The five cascades each had five vanes. A model of an aerodynamic grid was constructed by the shops out of wood blocks, for use in flow comparisons with the cascade models.

The vanes for each cascade, and for the grid, were then fastened with screws to a clear Plexiglas plate, which maintained the proper separation and orientation of the vanes. Clear Plexiglas was used to allow photography of the flow through the models with a shadowgraph. See Appendix B for sketches of the airfoils and of the grid cross-section used.

Optics

Visual observations and photographic recordings were made of the water flow patterns through the cascades, using a shadowgraph optical system. The system consisted of a light source, a spherical mirror, a flat mirror, and a paper screen taped to the underside of the water table. See Appendix D for a photograph of the system.

The light source, a mercury lamp and condenser lens combination, was located to the side of the test section. The 8-inch diameter, 71-inch focal length spherical mirror was located directly across the water table from the light source. The mirror, angled upward, reflected a parallel beam of light from the source to an 8-inch diameter flat mirror directly above the test section. The flat mirror was angled such that the light would be reflected down, through the test section, and onto the paper screen.

Alignment of the optics consisted of four steps: adjusting the distance between the lamp and condenser lens, so the light was focused by the lens on as small a point as possible; positioning the light source so that the lens focal point coincided with that of the spherical mirror; aiming the spherical mirror precisely at the flat mirror; adjusting the flat mirror in three dimensions so as to produce the best image on the screen of the cascade being tested. Because of the difficulty of this final adjustment, the mirror was attached to a camera tripod (the attachment

head of the tripod could be adjusted around three axes of rotation). The tripod was placed on the water table with the legs out of the way of the water flow through the test section.

The water flow through the test section could be observed visually from above or below the water table, and photographs were made from below. A 35mm SLR camera was used, with a 50mm lens and two types of film (Tri-X exposed at 800 ASA, and Ilford XP1-400 exposed at 1600 ASA).

Depth Measurements

Water depth measurements were made using a vertically translating pointed steel rod. Attached to the rod was an indicator which allowed measurements to the nearest hundredth inch on a steel rule. The rod was moved by turning a thumbwheel which bore against a frame made of aluminum angle with Plexiglas legs. The frame also had a set-screw and holder for the steel rule.

Measurements were made by first moving the rod down against the water table glass surface, and then by moving the rod until its point made contact with the water surface. Initial surface contact by the rod was noted by a dimpling of the water surface due to the water surface tension, or by surface tension waves set-up by the contact.

VI. Results

Shock Positioning

Each cascade was tested for its ability to keep the engine inlet shock positioned aft of the inlet throat, and forward of the point where the diffuser wall boundary layer thickened enough to grossly interfere with the shock. The cascade passages had a throat-to-cascade inlet area ratio that would cause flow choking at a specified cascade inlet Mach number. The results of this test were completely visual; a check was made on each cascade to insure that the inlet hydraulic jump never gained enough strength to produce the oblique shocks and boundary layer separation seen in Figure 5. The test was passed by *each cascade*.

Pressure Recovery

The differences among the cascade performances fell into the area of pressure recovery, and the determinants of pressure recovery were: cascade diffusion angle; vane angle-of-attack; radius ratio; the wall shapes of the cascade flow passages. The values for pressure recovery given in Table II should be considered carefully, with the following explanations in mind:

1. The pressure ratios were obtained by the hydraulic analogy, and were based on measured water depths. From Table I, $\left(P_a/P_f\right)_{air} = \left(D_a/D_f\right)^2_{water}$ with subscripts a and f denoting aft and forward of

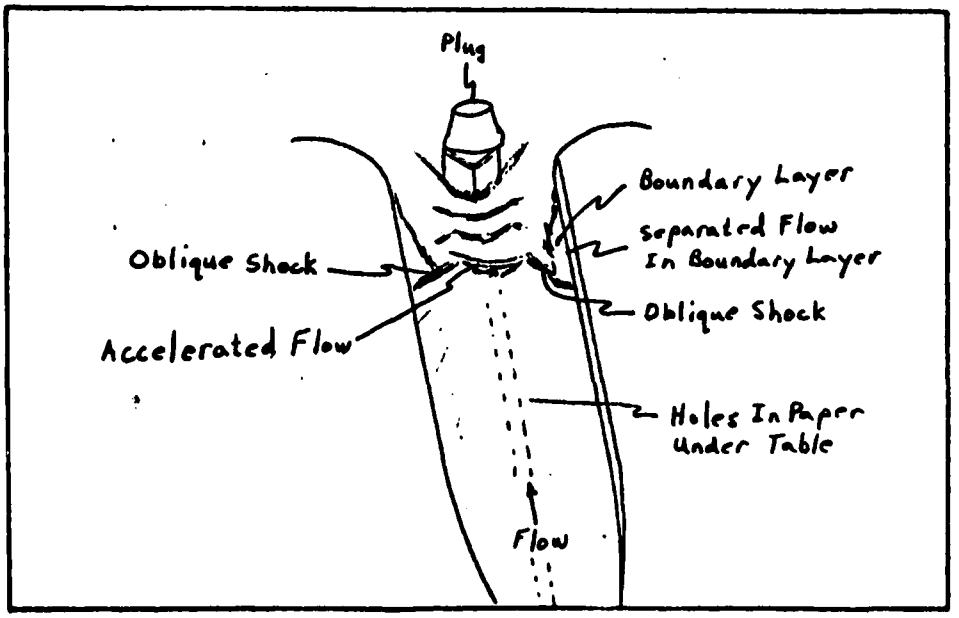

Figure 5 Diffuser Oblique Shock

Table II

Comparison and Performance of Cascade Designs

Design Number	Diffusion Angle	Solidity	R/D_h	Block	Unchoked P_a/P_t	Pipe Flow P_a/P_t	Remarks
1	10°	3.03	1.39	71%	0.84	0.80	Sharp corner at throat resulted in flow separation
1, $+10^\circ$ A-O-A	10°	3.03	1.39	71%	0.97	0.80	" " " "
2	20°	1.59	0.73	48%	0.77	0.70	Internal sharp turn
3	30°	1.59	0.73	48%	0.86	0.82	Smooth internal turn
4	40°	1.59	0.73	48%	0.76	0.68	Early flow separation in diffuser passages
5	7°	3.03	1.39	57%	0.92	0.90	Smooth internal turn
5, $+10^\circ$ A-O-A	7°	3.03	1.39	57%	0.92	0.90	" " "
Grid	12°	1.50	-	44%	0.93	0.93	Comparison grid

Pressures are static.
For cascade airfoils and the grid cross-section, see Appendix B.
An explanation of the pipe-flow calculation is in Appendix C.

the cascade, respectively. So, the accuracy of the pressure ratios depends on the accuracy of the depth measurements, and on where they were taken.

2. Some of the depth measurements were made in regions where surface waves allowed only approximate measurements.

3. The flow did not have a fully developed velocity profile anywhere in the tests in this study; and due to variations in water depth because of the different velocities in undeveloped flow along a cross-section, water depths presented as section-dependent (throat, forward of cascade, etc.) are actually point-dependent. The judgement of the experimenter was involved in selecting the depth measurement points which were to represent a particular cross-section.

The pressure ratios should not be taken as exact values, but should be compared among the cascades tested, as each was tested under similar conditions. A wooden model of the reference aerodynamic grid was tested for comparison to the cascades, and its test results are also found in Table II.

Radius Ratio. A large radius ratio was associated with better pressure recovery in this investigation. Contrast the results for cascades 2, 3, and 4 with the results for cascade 5 (see Table II). However, radius ratio is not the controlling factor in pressure recovery, as can be seen by comparing the results for cascades 1 and 3. The improvement in pressure recovery, if any, due to radius ratio was

probably overshadowed by other design factors.

Wall Shape. Refer to Appendix B for sketches of the airfoils and of the grid cross-section used in this investigation. The cascade passage wall shapes vary from those that give a smoothly turning flow (numbers 3, 4, and 5), to those that present the flow with sharp corners (number 1) or large turns to negotiate (number 2). There was no direct correlation between wall shape and pressure recovery, within the accuracy of the measurements. However, the photographs taken of flow through the cascades (see Appendix D) show that cascades number 1 and 2 suffer from more severe flow separation at the corners and hard turns than the other models suffer in their entire flow passages. Smooth curves and smooth changes in curvature were particularly important to the diffuser sections of the cascade passages. The diffuser sections were working under an adverse pressure gradient. An abrupt change in the wall curvature could have caused flow separation, as happened with cascades 1 and 2, when the cascade was supposed to be operating at its best pressure recovery. The best cascade, in terms of pressure recovery at zero angle-of-attack (number 5), was also the one with the smoothest wall shape.

Solidity and Blockage. Solidity and blockage did not have a clear effect on pressure recovery, either. The entire ranges of both solidity and blockage tested would be good for cascade designs, according to the test results. Still, it would be good to try and design cascades with as

large a radius ratio and as small a blockage as possible, to lengthen the effective radius of the turn and to reduce the wall friction as much as possible. See Table II.

Cascade Diffusion Angle. The cascade diffusion angle represents the rate at which an outlet passage (from throat to exit) of a cascade "opens up". This angle is the angle between a tangent to a point near the outlet edge of the upper surface of a vane, and a tangent to a point located on the under-surface of the vane on the same cross-section (see Figure 6). The diffusion angle is an indicator of how much the flow has to turn, within the cascade, against an adverse pressure gradient. In looking at Table II, it can be seen that there can be no direct correlation drawn between diffusion angle and pressure recovery. However, the cascade with the best recovery (number 5) has the smallest diffusion angle, and the cascade with the worst recovery (number 4) has the largest diffusion angle. Diffusion angle did have an effect on whether or not an increase in vane angle-of-attack was effective in reducing the size of the turbulence zone after a turn.

Angle-of-Attack. Three of the cascades, numbers 1, 4, and 5, were tested with the angles-of-attack of their vanes increased. As a result, the turbulent zone on the inner wall after the turn disappeared in the test of cascades 1 and 5. The zone shrank slightly with cascade number 4, but did not disappear. The separated area of flow on the rear suction sides of the vanes in number 4 (due to the large

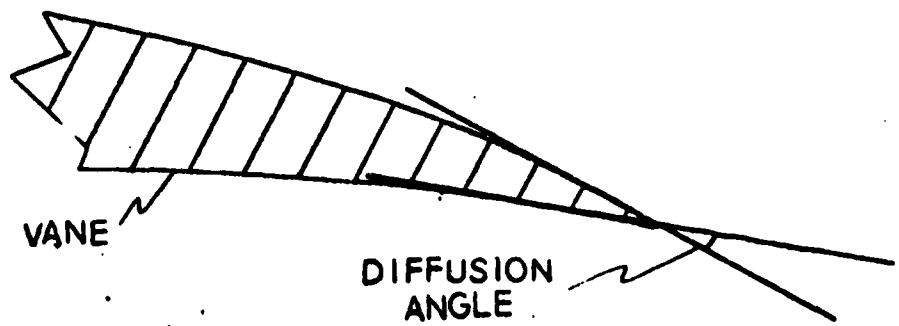

Figure 6 Cascade Diffusion Angle

divergence angle) was increased in size. This negated any effect that the cascade downwash had on the turbulent zone. So, it appears that increased vane angle-of-attack only helps in cascades that have almost no flow separation from the vanes at zero angle-of-attack (those with smooth wall curvatures and low diffusion angles).

Pipe Flow. A comparison was done to check the calculated pressure ratios versus a pipe flow analysis of the same system, for possible use in the design process (see Appendix C). Admittedly, it was an approximate analysis, but it allowed a check for order-of-magnitude errors and a check of trends. The pipe flow model is fully developed, steady, and in straight ducts of constant cross-sectional area. The test flow was none of these (Ref 8: 1,2). However, there was a correlation, as can be seen from comparing the columns of Table II.

VII. Conclusions and Recommendations

Conclusions

This study showed that a flow-controlling cascade turn can be designed to accomplish the shock positioning function and to have a pressure recovery comparable to that of an aerodynamic grid. The study also proved the utility of the water table in preliminary testing of these cascades, and in flow visualization.

The shock positioning function was accomplished by all of the cascades.

The pressure recovery was a function of the cascade diffusion angle, the individual vane angle-of-attack, and to some extent the curvature of the vane surfaces. Giving the vanes a small amount of positive angle-of-attack improved the pressure recovery of two cascades with small diffusion angles, but did not improve the recovery of one with a large diffusion angle. The curvature of the vane surfaces was important in determining the point(s) where flow separation occured, and in how abruptly the incoming flow had to adjust to the conditions imposed by the cascade. The pressure recovery was better for a cascade with a forebody that had no abrupt changes in curvature, than for a cascade with such changes. So, the factors which lead to the best pressure recovery were smooth wall curvatures, small diffusion angles, large radius ratios, and medium amounts of blockage.

Recommendations

Based on this study, it is recommended that work be done in gas dynamic tests of shock positioning, flow turning cascades, using the designs from the study as starting points. The gas dynamic work would allow validation of the concepts in shock positioning and pressure recovery put forth in this study.

The pipe flow analysis described herein needs gas dynamic validation, as it could be a good tool for estimating the pressure recovery of turning cascade designs before they are constructed. Further work in the AFIT blow-down wind tunnel or low pressure shock tube would accomplish the validation task, and possibly provide the Air Force with hardware designs useful in ramjet-powered vehicles.

Bibliography

1. Bruce, Philip W. Flow Visualization in Axial-Flow Compressor and Turbine Cascades Utilizing the Water Table. MS thesis. Wright-Patterson AFB, Ohio: Air Force Institute of Technology, December 1973. (GAM/AE/73A-3).

2. Daugherty, Robert L. and Franzini, Joseph B. Fluid Mechanics with Engineering Applications (Seventh Edition). New York: McGraw-Hill Book Company, 1977.

3. Hill, Phillip G. and Peterson, Carl R. Mechanics and Thermodynamics of Propulsion. Reading, Massachusetts: Addison-Wesley Publishing Company, 1970.

4. Huzel, Sieter K. et al. Design of Liquid Propellant Rocket Engines (Second Edition). Washington: National Aeronautics and Space Administration, 1971. (N71-29405-416).

5. Ideuchik, I.B. Handbook of Hydraulic Resistance--Coefficients of Local Resistance and of Friction. Translation from Russian by the Israel Program for Scientific Translation, Jerusalem, 1966. Moscow-Leningrad: 1960.

6. Russell, George E. Hydraulics (Fifth Edition). New York: Henry Holt and Company, Inc., 1946.

7. Shapiro, Ascher H. The Dynamics and Thermodynamics of Compressible Fluid Flow. New York: John Wiley and Sons, 1953.

8. Shapiro, Ascher H. and Smith, R.D. Friction Coefficients in the Inlet Length of Smooth Round Tubes. TN-1785. Washington: National Advisory Committee for Aeronautics, November 1948.

9. Thomas, Arthur N., Jr. Efficient Flow Distribution Control by Means of an Aerodynamic Grid. Van Nuys, California: The Marquardt Company, August 1962.

10. Truly, Richard H., Jr. et al. Supersonic Diffuser with Shock Positioning Means. Washington: United States Patent Office, Patent Number 2,968,147. Patented 17 January 1961.

11. Turchetti, A.J. and Robertson, J.M. Design of Vaned-Turns for a Large Water Tunnel. Paper Number 48-SA-15. Presented to the Semi-Annual Meeting of the ASME, 30 May - 4 June 1948. New York: American Society of Mechanical Engineers, 1948.

Appendix A

Cascade Design

The criteria used in this study for the design of a cascade were:

1. The determining factor for whether or not guide vanes should be used in a turn is the ratio R/D_h: for a constant area turn, $R/D_h \leq 0.4$ to 0.5 calls for vanes; for a diffusing turn, $R/D_h \leq 1.0$ calls for vanes; for a reducing turn, $R/D_h \leq 0.2$ calls for vanes (Ref 5:201-203).

2. Mach 1 at the passage throats when Mach 0.465 is reached at the passage inlets. So, $B/S = 1.365481874$.

3. Reynolds number of 100,000, based on the smallest orifice dimension, as a minimum. This Reynolds number cannot be matched on the water table, but it is still a design factor. For example: assuming the Reynolds number is matched, what characteristic length is needed for a water model to correspond to an air model?

$$R_{e_{air}} = R_{e_{water}}, \qquad R_e = VL/\nu$$

so $L_{air}/L_{water} = V_{water}\,\nu_{air}/V_{air}\,\nu_{water}$

At 60 F, sea level- $\nu_{air} = 1.564 \times 10^{-4}\ ft^2/s$

$\nu_{water} = 1.217 \times 10^{-5}\ ft^2/s$

For $M = F = 1$ - $V_{air} = A_s = \sqrt{KR_gT} = 1337\ ft/s$

$V_{water} = C = \sqrt{GD} = 1.55\ ft/s$ @ $D = 0.9\ in$

$L_{air}/L_{water} = 0.015$

for a critical grid dimension (that of an individual

flow passage opening) of 0.0183ft, L_w = 1.22ft. Considering that the cascade will have at least four passages, the water table is not large enough to handle such a model. Even with water at its boiling point, L_w = 0.32ft. This is still too large, when the vane thickness for such a model is included.

4. Turn angle of 90°, so $\ell = R/\sin \theta/2 = R/\sin 45°$

5. Number of vanes, $n = 2.13\,(D_h/R) - 1$ (Ref 5: 200-201).

6. Spacing of vanes, $B = m/n+1$. Check that $R/D_h \leq$ 0.4 to 0.5.

7. Consider using a 2% trailing edge "droop", to account for boundary layer narrowing of the flow passage.

8. Desired solidity, ℓ/s.

   a) A low solidity means wide vane spacing, and a higher lift per vane.

   b) A high solidity means narrow vane spacing and lower lift per vane, but it also means larger losses due to blockage and friction.

9. Note that all these conditions, given D_h , overspecify the design. Only one solidity is possible:

$$R = \ell \sin 45°$$

$$n = 2.13\,(D_h/R) - 1 = 2.13\,(D_h/\ell \sin 45°) - 1$$

$$B = m/n+1 = m/\{2.13\,(D_h/\ell \sin 45°) - 1 + 1\} = \frac{\ell m \sin 45°}{2.13\, D_h}$$

$$s = B/1.365 = \ell m \sin 45°/1.56\, D_h$$

$$\therefore \ell/s = 2.21\, D_h/m$$

If the duct is rectangular, $D_h = 4 \times \text{Area}/\text{Perimeter}$

$$D_h = \frac{4}{2} \times \frac{\text{Length} \times \text{Width}}{\text{Length} + \text{Width}}$$

$$m = \text{Width}/\cos 45^\circ$$

So, m depends on D_h, and if D_h is given, l/s is specified.

It was decided that criteria numbers 2, 3, 6, 7, and 8 were the critical ones, and that the others could be adjusted slightly to allow for changes in solidity.

Another factor not considered in this study, but one that must be carefully considered in the actual design of a cascade for an engine, is the number of vanes. It will have an impact on how close to the combustor flameholders or dump region a cascade can be placed. The fewer the vanes, the farther upstream the cascade will have to go, to allow a uniform flow velocity profile in the duct prior to the combustor.

With the above design factors in mind, the layout of the vane cross-sections was relatively simple (see Appendix B). On a sheet of graph paper, a 90° arc of a circle the proper radius was drawn to be either the vane underside or a guide for the vane drawing. Another arc was laid out above the first, with their centers of curvature H distance apart. Then a compass, set to the distance S, was used to scribe out the passage throat height. See Figure A-1. Next, the distance B (and B', if a 2% allowance for boundary layer effects was included) was laid out, and the remainder of the upper surface was filled in with a French curve.

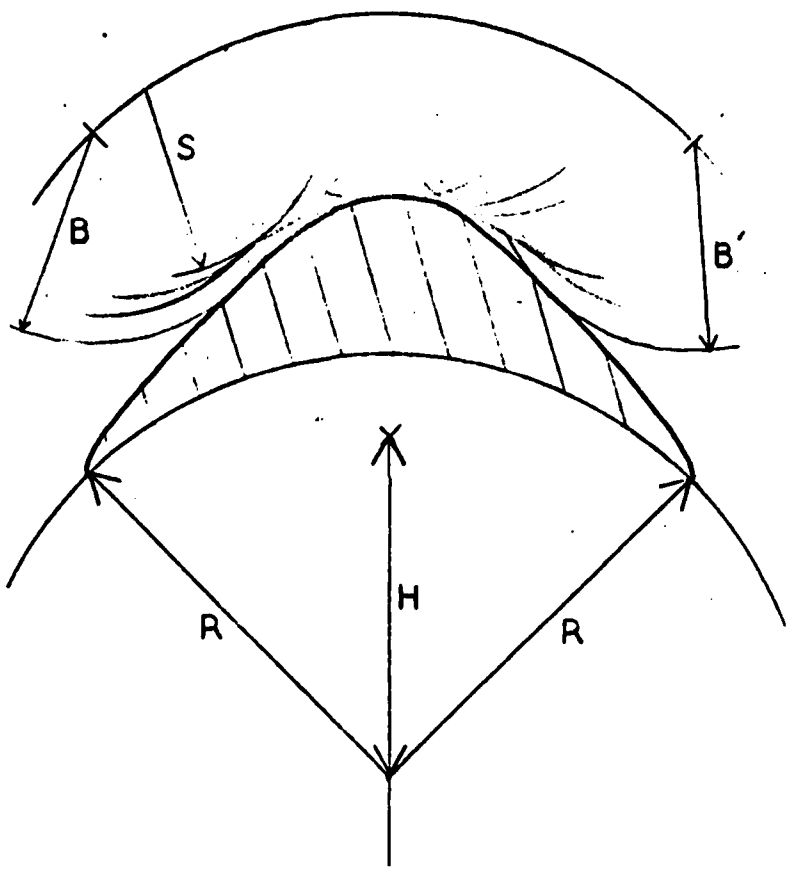

Figure A-1 Vane Layout

Appendix B

Vane Cross-Sections

On the following pages will be found the airfoil sections used in this study. The grid model cross-section is also included. All of the drawings are to scale for the models used on the water table.

Cascade 1 was designed to be a convergent-divergent nozzle, bent around a 90° turn, and to have a small diffuser divergence angle. Note the sharp corner at the throat, which was a result of the combination of blockage and solidity chosen.

Cascade 2 was also designed to be a C-D nozzle, bent around a 90° turn. In order to have no sharp corners internally, smaller solidity, blockage, and a smaller radius ratio than in the design of number 1 were chosen. It has a diffusion angle larger than that of number 1, but smaller than those of numbers 3 or 4.

Cascade 3, a curved C-D nozzle, was designed to have a smoother, less sharp internal turn than number 2. It has the same solidity, blockage, and radius ratio as cascades number 2 and 4, but its diffusion angle is midway between those of numbers 2 and 4.

Cascade 4 has a semi-blunt forebody, and the largest diffusion angle of all the cascades in this study. It turns the flow more in its diffuser sections, and less in its forebody passages, than any other cascade in this study.

Cascade 5 was designed to incorporate the best qualities of the other four designs. It has the smallest diffusion angle, smooth internal turns, relatively small blockage, a large radius ratio, and is a curved C-D nozzle.

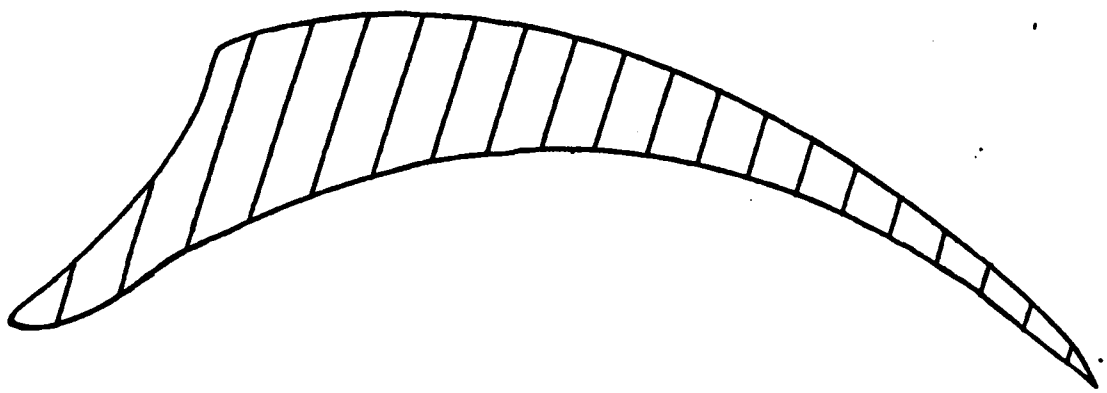

Figure B-1 Cascade 1

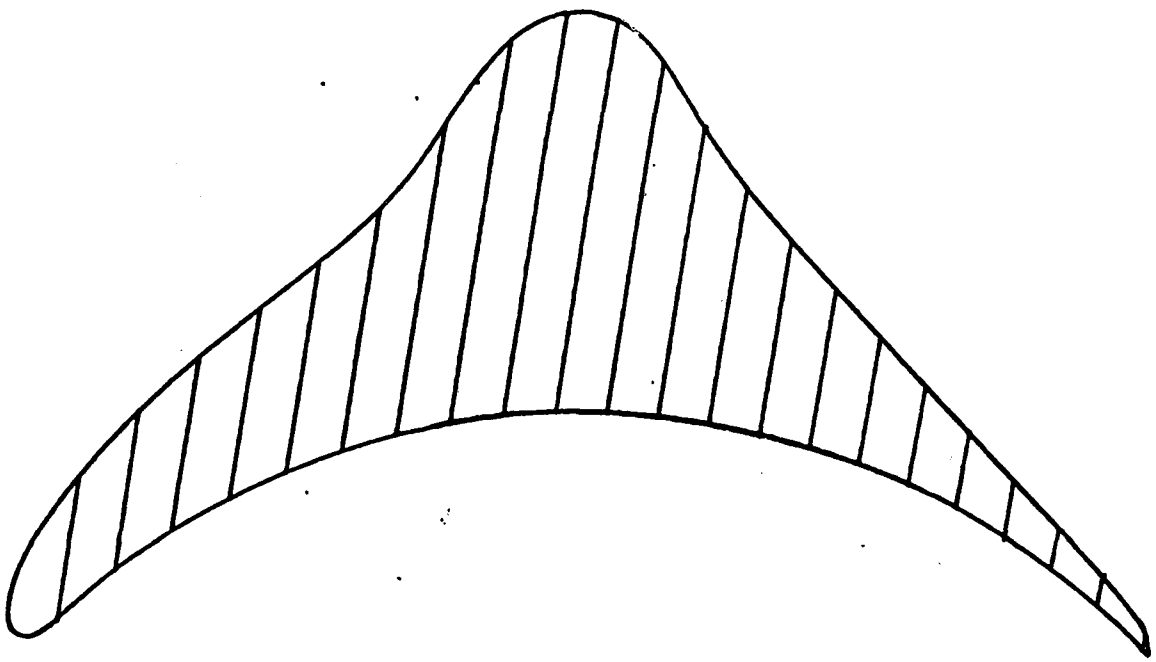

Figure B-2 Cascade 2

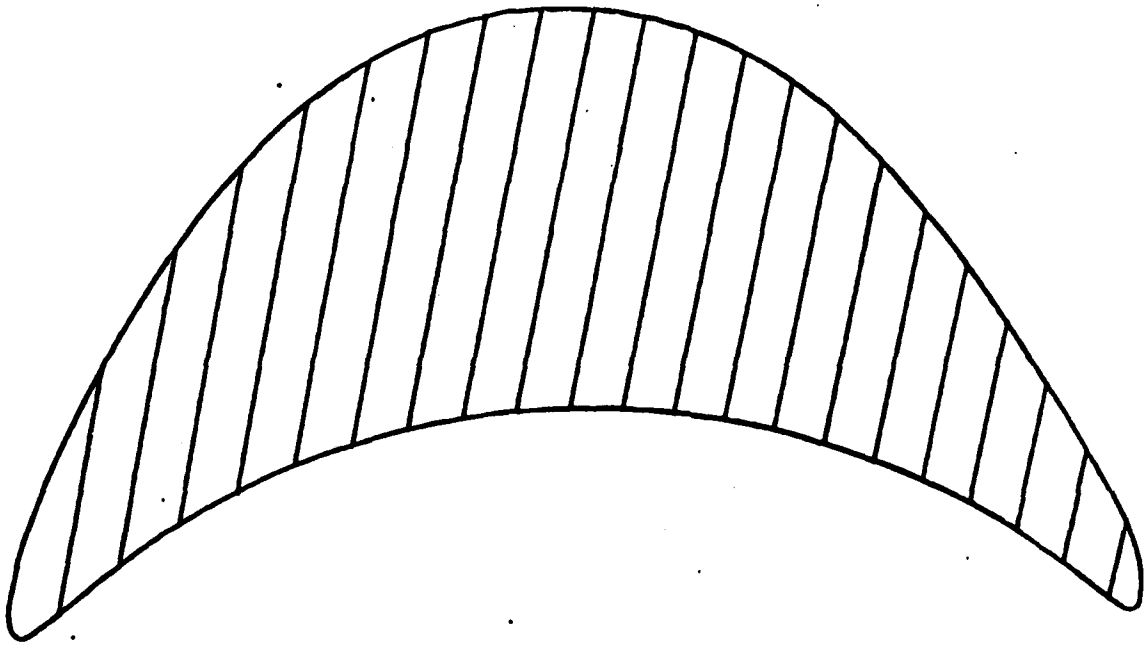

Figure B-3 Cascade 3

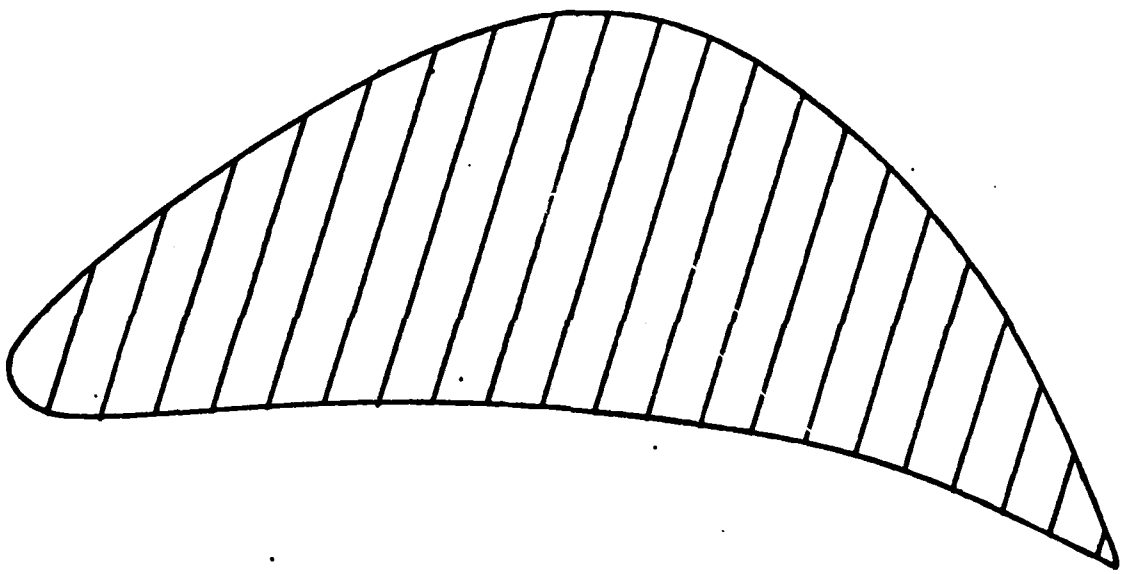

Figure B-4 Cascade 4

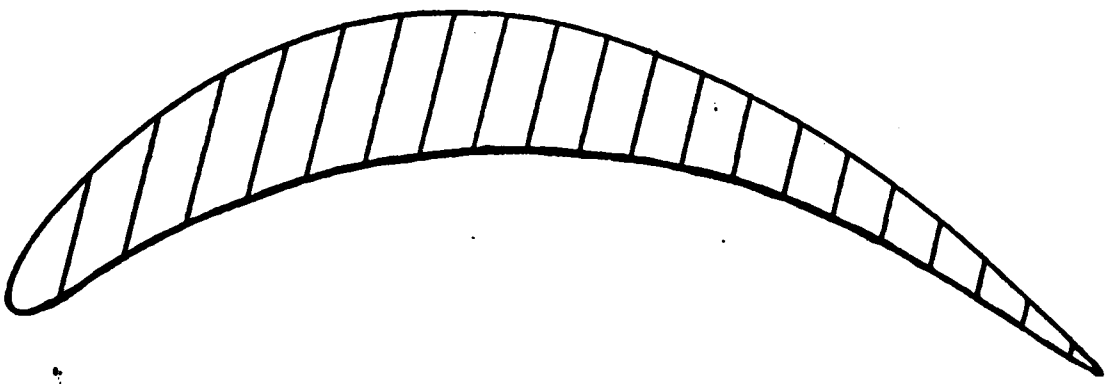

Figure B-5 Cascade 5

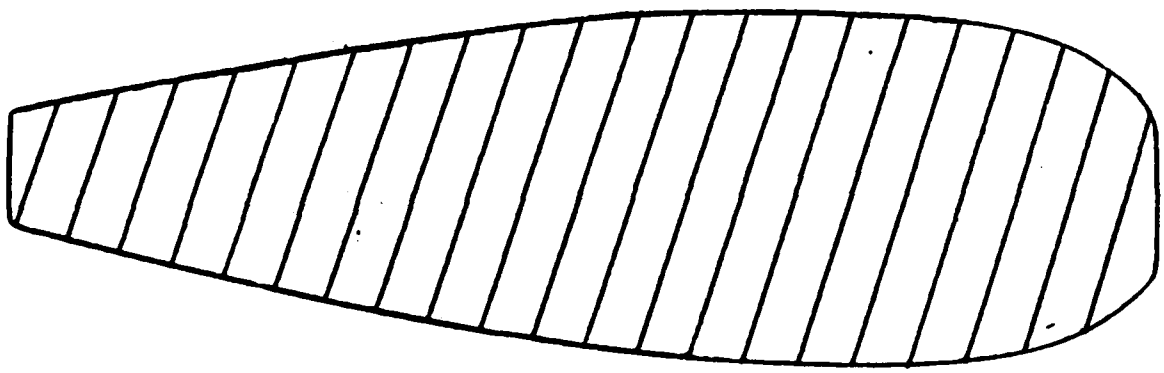

Figure B-6 Aerodynamic Grid

Appendix C

Pipe Flow Analysis

In an effort to find the static pressure loss across each cascade when working under conditions for optimum pressure recovery, an analysis of the fluid flow through a cascade passage was done as if the flow were fully developed and in a duct of constant cross-sectional area. The values obtained were then compared to measured static pressure losses, which were derived through the hydraulic analogy. See Figure C-1 for a flow chart of the pressure ratio calculation.

The surface roughness, ε, of each cascade model and of the grid model, was measured with a profilometer. The models all had roughnesses on the order of 0.0004 ft.

The roughness of each cascade was divided by the hydraulic diameter, D_h, of the smallest cross-section of a passage from the particular cascade model, to get the ratio ε/D_h. The Reynolds number of each passage was determined by the use of the kinematic viscosity of water at 80 F, the passage hydraulic diameter of the water table model, and the velocity of water through the passage. The velocity was obtained through the hydraulic analogy (using Table I), the water height, and the local Froude number from the particular test involved in the calculation. Then, the relative roughness, ε/D_h, and the Reynolds number were used as entering arguments in a Moody diagram to find the D'Arcy

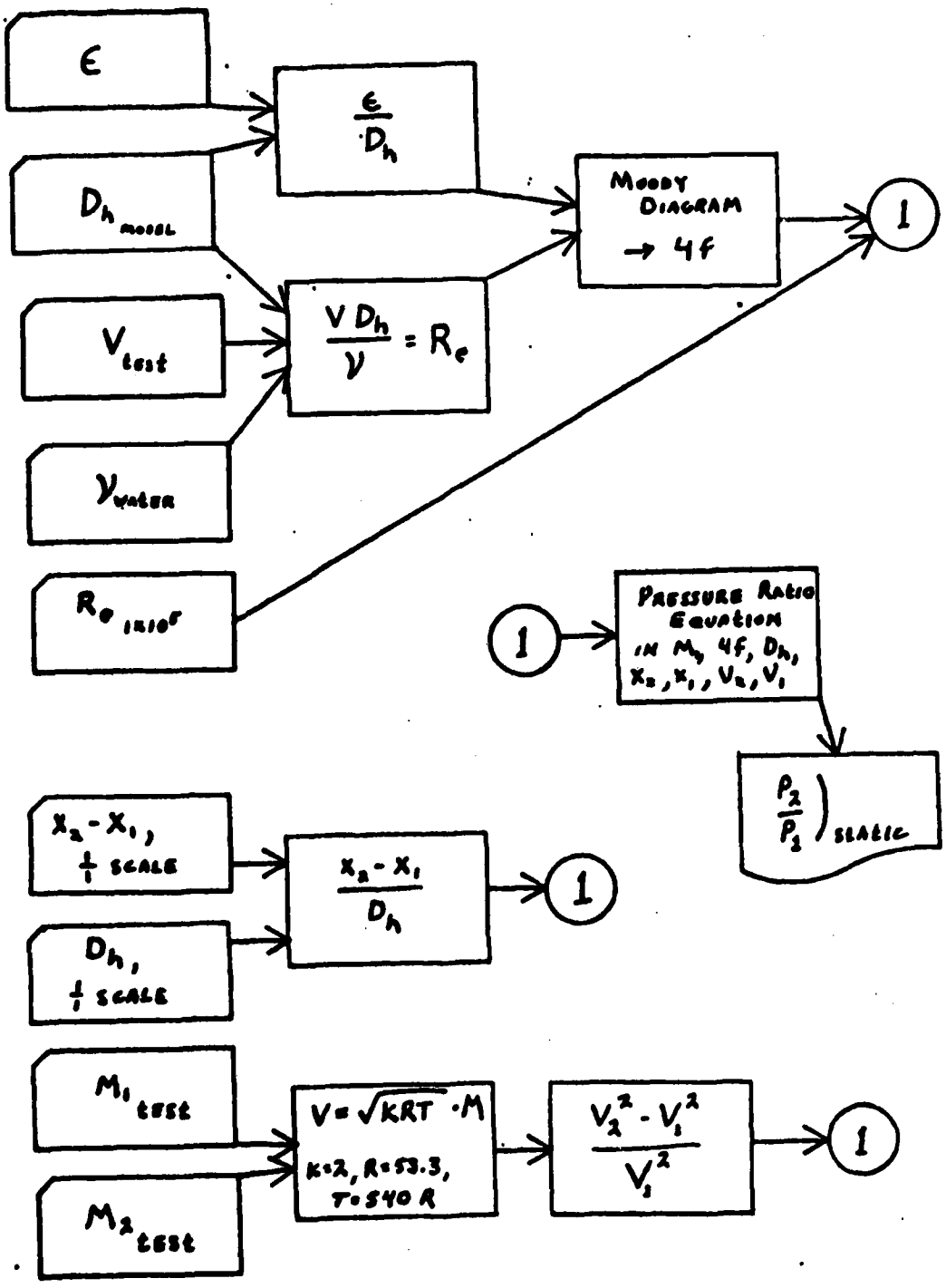

Figure C-1 Flow Chart of Pipe Flow Calculations

friction factor, $4f$ (Ref 2: 214,215,539).

For a perfect gas, with steady and adiabatic flow, the following equation relates static pressure change, velocity change, area change, and friction:

$$-\left(\frac{KM^2}{1-M^2}\right)\left(1-\frac{KM^2}{1+\{K-1\}M^2}\right)\frac{dA}{A}+\frac{dP}{P}-\frac{KM^2}{2}\frac{dV^2}{V^2}+\frac{KM^2}{2}4f\frac{dx}{D_h}=0$$

(Ref 7: 231)

In general, $dy=\lim_{h\to 0}\Delta y/h$, where h is the distance between two points in the domain of $y=f(x)$. $dy\cong\Delta y$, with the closeness of the approximation depending on the distance between the two points being examined in the domain of y. So,

$$-\left(\frac{KM^2}{1-M^2}\right)\left(1-\frac{KM^2}{1+\{K-1\}M^2}\right)\frac{\Delta A}{A}+\frac{\Delta P}{P}-\frac{KM^2}{2}\frac{\Delta(V^2)}{V^2}+\frac{KM^2}{2}4f\frac{\Delta x}{D_h}=0$$

$\Delta A\cong 0$, because the inlet and outlet of the cascade have the same cross-sectional area. Let us examine the function around point 1, the inlet of the cascade, and assume that point 2, the outlet of the cascade, is not functionally very distant from point 1:

$$\frac{\Delta P}{P_1}-\frac{KM_1^2}{2}\frac{\Delta(V^2)}{V_1^2}+\frac{KM_1^2}{2}\frac{4f}{D_h}\Delta x=0$$

$$\frac{P_2-P_1}{P_1}+\frac{KM_1^2}{2}\left\{\frac{4f}{D_h}(x_2-x_1)-\frac{V_2^2-V_1^2}{V_1^2}\right\}=0$$

$$\therefore\ \frac{P_2}{P_1}=1-\frac{KM_1^2}{2}\left\{\frac{4f}{D_h}(x_2-x_1)-\frac{V_2^2-V_1^2}{V_1^2}\right\}$$

This equation was used to calculate the pressure ratio across a cascade, by substituting the $4f$ value derived, above, for pipe flow in a cascade passage. In addition, $4f$

for a Reynolds number of 100,000 was found. This friction factor was obtained for comparison (it is supposed to be the minimum for an aerodynamic grid orifice under actual operating conditions) to the friction factor obtained in the water test, to see if wall friction calculated in this manner had much of an effect on the static pressure ratio. As can be seen in Table C-1, the friction factors calculated from the water tests were about 30% larger than those from the Reynolds number of 100,000. However, the static pressure ratios calculated from each factor were the same out to two decimal places. So, in this comparison, the wall friction factor does not have much impact on the static pressure ratio.

In the pressure ratio equation, X_2-X_1 was the average path length a fluid particle would flow through a $\frac{1}{1}$-scale cascade, and D_h was the hydraulic diameter of a $\frac{1}{1}$-scale cascade. V_1 and V_2 were calculated by converting water-test Mach numbers ahead and behind the cascades to velocities in air at sea-level and 80 F.

So, the friction factor was determined from water flow conditions, but the remainder of the problem was modeled after postulated "actual" conditions. The results of the calculations can be found in Table C-1.

Table C-1

Calculated Static Pressure Ratios

Cascade	$D_h)_{water}$	ϵ/D_h	$V_1)_{water}$	$Re \times 10^3$	$4f)_{water}$	$4f)_{Re=10^5}$	$D_h)_{sim}$	$(X_2-X_1)_{sim}$	$V_1)_{sim}$	$V_2)_{sim}$	M_1	$P_2/P_1)_{water}$	$P_2/P_1)_{Re=10^5}$
1	.924	.0052	.82	6.78	.0405	.031	.507	1.39	504	776	.37	.80	.80
2	1.26	.0038	.46	5.19	.041	.0259	.392	.73	354	817	.26	.70	.70
3	1.26	.0038	.52	5.87	.0395	.0259	.392	.73	449	722	.33	.82	.82
4	1.26	.0038	.62	7.00	.038	.0259	.392	.73	504	913	.37	.68	.68
5	1.00	.0048	.69	6.18	.040	.030	.424	1.39	518	654	.38	.90	.90
Grid	1.34	.0036	.53	6.36	.0395	.0258	.393	.481	463	586	.34	.92	.93

All calculations used a kinematic viscosity (for Re) of 0.930×10^{-5} ft^2/s (80F).
X_2-X_1 in this table is the average path length that a fluid particle would follow through a cascade passage.
D_h is in inches; $V_1)_{w}$ is in ft/s; X_2-X_1 is in inches; $V_1)_{sim}$ and $V_2)_{sim}$ are in ft/s.

Appendix D

Photographs

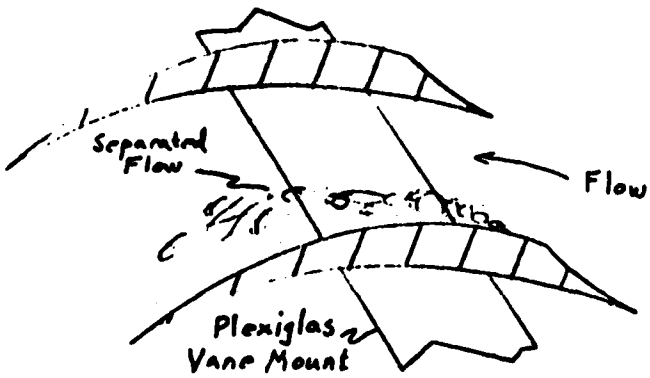

Figure D-1 Cascade 1, Optimum Inlet Pressure Recovery

Figure D-2 Cascade 1, Cascade Choked

Figure D-3 Cascade 2, Optimum Inlet Pressure Recovery

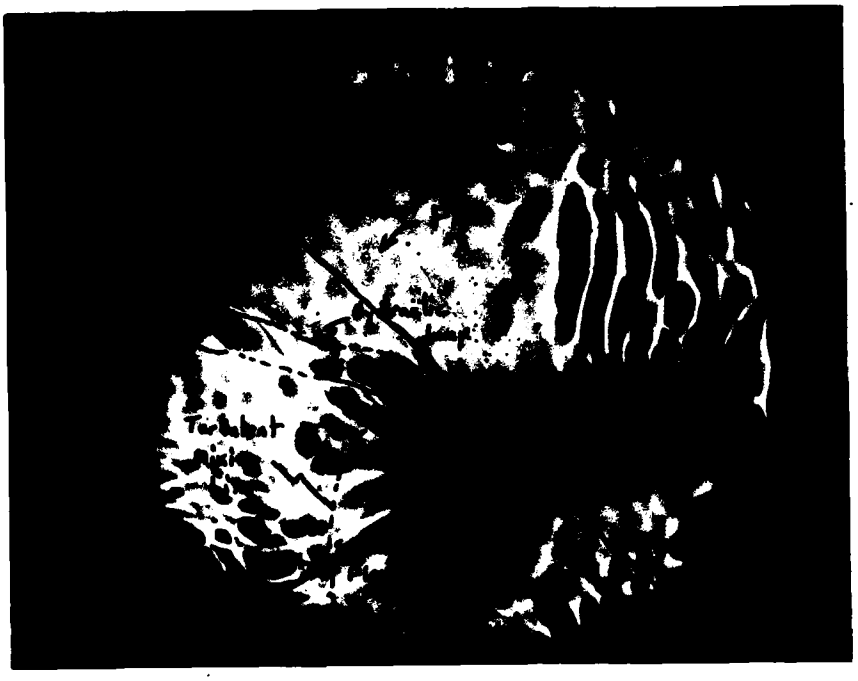

Figure D-4 Cascade 2, Cascade Choked

Figure D-5 Cascade 2 From Above, Showing Vertical Flow Accelerations

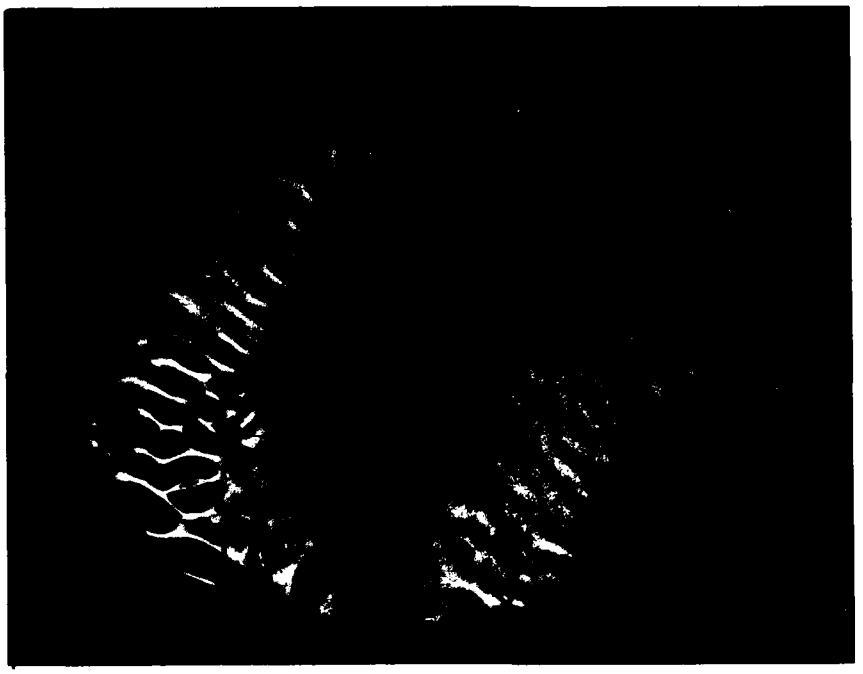

Figure D-6 Cascade 3, Optimum Inlet Pressure Recovery

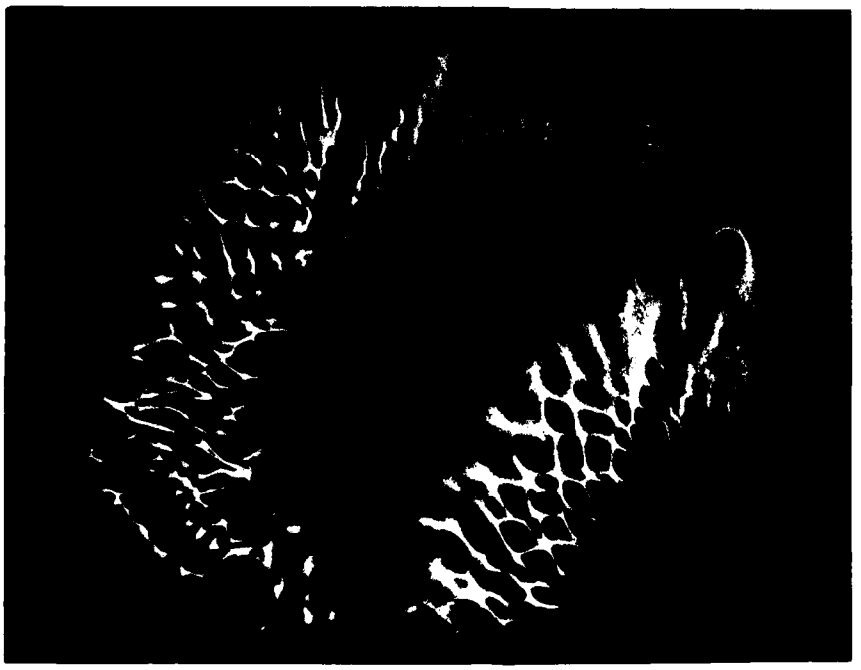

Figure D-7 Cascade 3, Cascade Choked

Figure D-8 Cascade 3 From Above, Showing Vertical Flow Accelerations

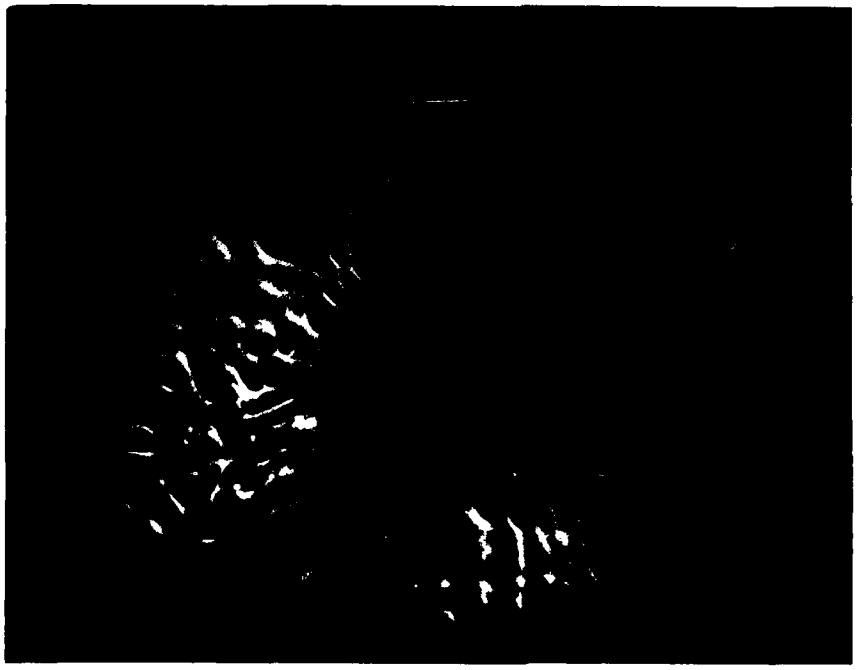

Figure D-9 Cascade 4, Optimum Inlet Pressure Recovery

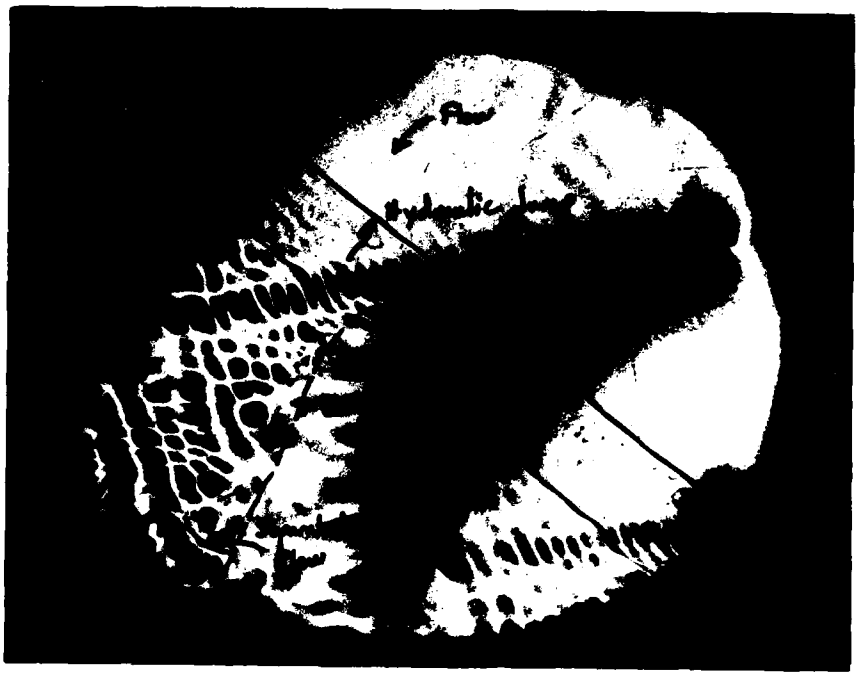

Figure D-10 Cascade 4, Cascade Choked

Figure D-11 Cascade 4 From Above, Showing Vertical Flow Accelerations

Figure D-12 Cascade 5, Optimum Inlet Pressure Recovery

Figure D-13 Cascade 5, Cascade Choked

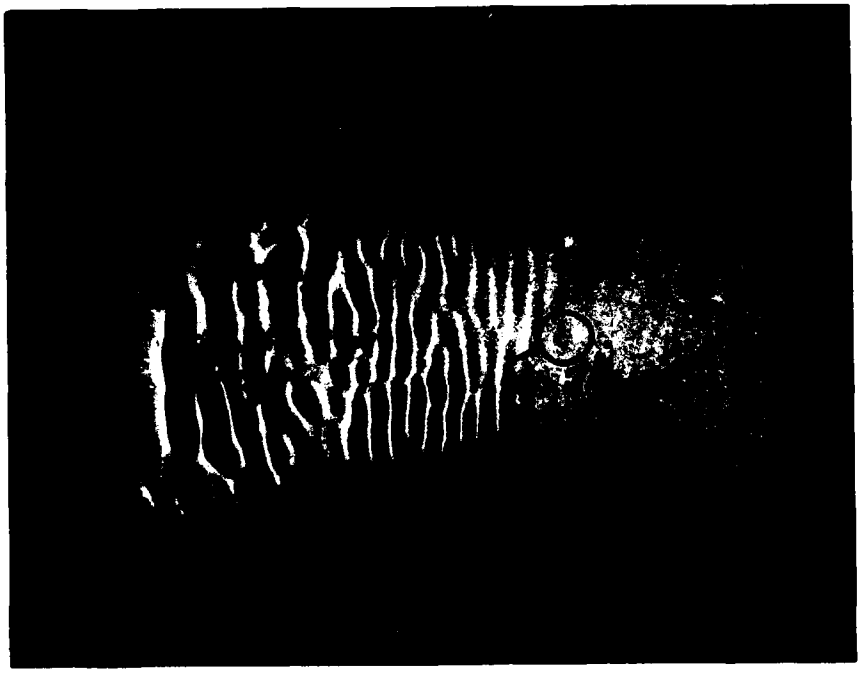

Figure D-14 Grid, Optimum Inlet Pressure Recovery

Figure D-15 Grid Choked

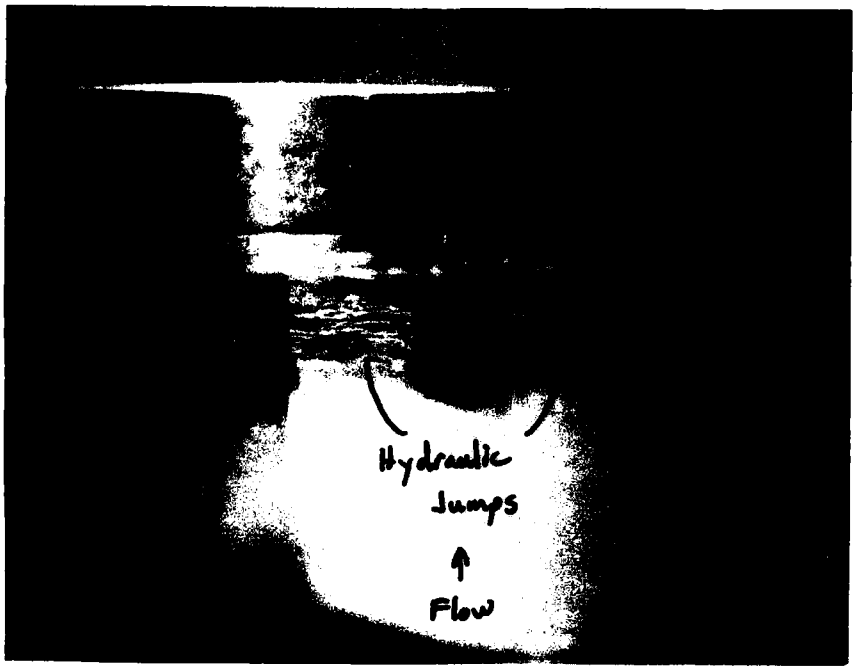

Figure D-16 Grid From Above, Showing Hydraulic Jumps

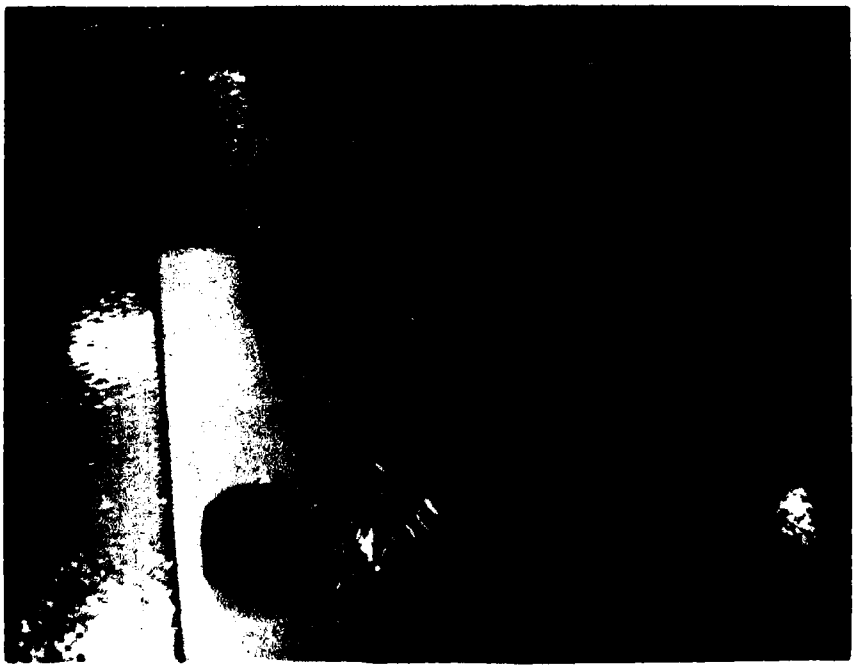

Figure D-17 Normal Hydraulic Jump in Inlet

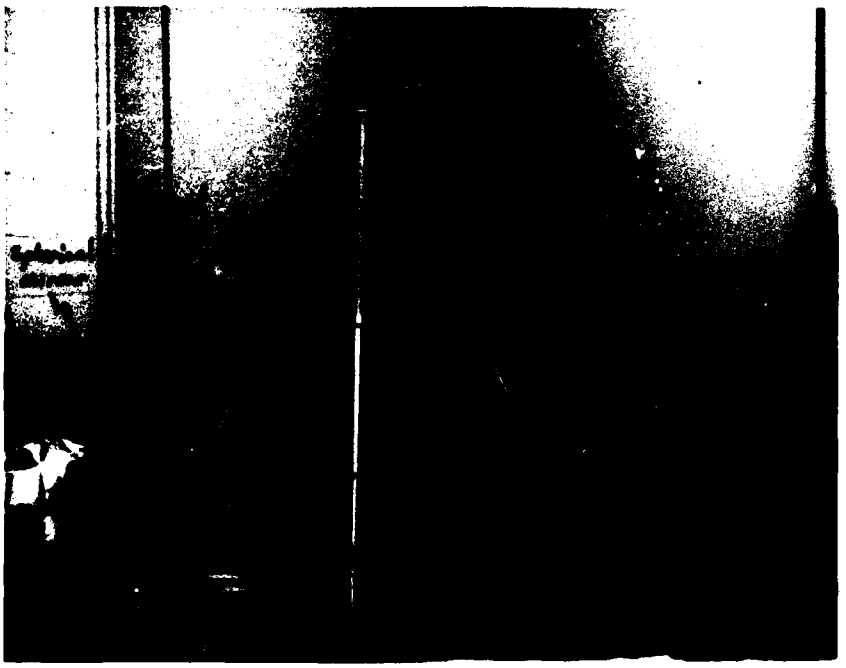

Figure L-18 Experimental Set-Up

VITA

Jason Baird was born 23 December 1955 at Ramey AFB, Puerto Rico. He graduated from high school in Mountain Grove, Missouri, in 1974 and attended the United States Air Force Academy from which he received the degree of Bachelor of Science in Engineering Sciences in May 1978. He completed navigator training and received his wings in January 1979. He then served as a B-52H navigator in the 46th Bomb Squadron, and as an air operations staff officer in the 319th Bomb Wing, Grand Forks AFB, North Dakota, until entering the School of Engineering, Air Force Institute of Technology, in June 1981.

Permanent address: Route 2
Norwood, Missouri 65717

UNCLASSIFIED

SECURITY CLASSIFICATION OF THIS PAGE (When Data Entered)

REPORT DOCUMENTATION PAGE

READ INSTRUCTIONS BEFORE COMPLETING FORM

1. REPORT NUMBER: AFIT/GAE/AA/82D-3

2. GOVT ACCESSION NO.: AD-A124782

3. RECIPIENT'S CATALOG NUMBER:

4. TITLE (and Subtitle): DESIGN OF CHOKING CASCADE TURNS

5. TYPE OF REPORT & PERIOD COVERED: MS Thesis

6. PERFORMING ORG. REPORT NUMBER:

7. AUTHOR(s):

8. CONTRACT OR GRANT NUMBER(s):

9. PERFORMING ORGANIZATION NAME AND ADDRESS:
Air Force Institute of Technology
(AFIT-EN)
Wright-Patterson AFB, OH 45433

10. PROGRAM ELEMENT, PROJECT, TASK AREA & WORK UNIT NUMBERS:

11. CONTROLLING OFFICE NAME AND ADDRESS:
Ramjets Division, Air Force Wright
Aeronautical Laboratory (AFWAL/PORA)
Wright-Patterson AFB, OH 45433

12. REPORT DATE: December 1982

13. NUMBER OF PAGES:

14. MONITORING AGENCY NAME & ADDRESS (if different from Controlling Office):

15. SECURITY CLASS. (of this report): Unclassified

15a. DECLASSIFICATION/DOWNGRADING SCHEDULE:

16. DISTRIBUTION STATEMENT (of this Report):
Approved for public release; distribution unlimited

17. DISTRIBUTION STATEMENT (of the abstract entered in Block 20, if different from Report):

18. SUPPLEMENTARY NOTES:
Approved for public release: IAW AFR 190-17.
LYNN E. WOLAVER
Dean for Research and Professional Development
Air Force Institute of Technology (ATC)
Wright-Patterson AFB OH 45433
6 JAN 19

19. KEY WORDS (Continue on reverse side if necessary and identify by block number):
Aerodynamic Grid
Ramjet Engine Inlets
Inlet Shock-Positioning
Hydraulic Analogy
Water Table (or Tunnel)

20. ABSTRACT (Continue on reverse side if necessary and identify by block number):
Five different shock-positioning cascades, for short-radius turns in ramjet inlet diffusers, were designed and tested on the AFIT water table. These flow controllers were to perform the same function as the conventional arrangement of an aerodynamic grid and a long-radius turn. The tests were to determine the suitability of the water table for such experimentation, in addition to determining the flow-control capabilities and pressure recovery of the cascades. All five

DD FORM 1 JAN 73 1473 EDITION OF 1 NOV 65 IS OBSOLETE

UNCLASSIFIED

SECURITY CLASSIFICATION OF THIS PAGE (When Data Entered)

designs accomplished the flow-control function as designed, and two designs exhibited the same or better pressure recovery than the aerodynamic grid. The water table proved to be an excellent means of testing these cascades, primarily due to the ease of flow visualization in the tests done. The shock-positioning cascade, short-radius turn concept shows promise and should be tested further in gas-dynamic apparatus.

END

FILMED

3-83

DTIC